IOP Publishing Smart Materials and Structures
Smart Mater. Struct. 24 (2015) 115005 (13pp) doi:10.1088/0964-1726/24/11/115005

Energy harvesting from controlled buckling of piezoelectric beams

M H Ansari and M Amin Karami

Department of Mechanical and Aerospace Engineering, University at Buffalo (SUNY), New York, USA

E-mail: mansari2@buffalo.edu

Received 12 June 2015, revised 7 August 2015
Accepted for publication 24 August 2015
Published 25 September 2015

Abstract

A piezoelectric vibration energy harvester is presented that can generate electricity from the weight of passing cars or crowds. The energy harvester consists of a piezoelectric beam, which buckles when the device is stepped on. The energy harvester can have a horizontal or vertical configuration. In the vertical (direct) configuration, the piezoelectric beam is vertical and directly sustains the weight of the vehicles or people. In the horizontal (indirect) configuration, the vertical weight is transferred to a horizontal axial force through a scissor-like mechanism. Buckling of the beam results in significant stresses and, thus, large power production. However, if the beam's buckling is not controlled, the beam will fracture. To prevent this, the axial deformation is constrained to limit the deformations of the beam. In this paper, the energy harvester is analytically modeled. The considered piezoelectric beam is a general non-uniform beam. The natural frequencies, mode shapes, and the critical buckling force corresponding to each mode shape are calculated. The electro-mechanical coupling and the geometric nonlinearities are included in the model. The design criteria for the device are discussed. It is demonstrated that a device, realized with commonly used piezoelectric patches, can generate tens of milliwatts of power from passing car traffic. The proposed device could also be implemented in the sidewalks or integrated in shoe soles for energy generation. One of the key features of the device is its frequency up-conversion characteristics. The piezoelectric beam undergoes free vibrations each time the weight is applied to or removed from the energy harvester. The frequency of the free vibrations is orders of magnitude larger than the frequency of the load. The device is, thus, both efficient and insensitive to the frequency of the force excitations.

Keywords: vibration energy harvesting, bimorph piezoelectric beams, controlled buckling, car energy harvesting, shoe energy harvesting

(Some figures may appear in colour only in the online journal)

1. Introduction

In recent years, energy harvesting devices have attracted significant interest in industrial and manufacturing sectors. The unique ability of converting ambient energy into electrical energy has motivated several academic and commercial groups to be involved in the analysis and development of energy harvesting technology. Commonly, the generated electricity is stored in capacitors or batteries. For more information on vibration energy harvesting in general the reader may refer to [1–3]. Specifically, bridge vibrations can be converted to electricity to power structural health monitoring sensor nodes, traffic sensors, or possibly road signs [4–7]. In this method, the energy originates from the passing vehicles, translates to the bridge and causes vibrations in the bridge. This vibration is converted into electrical energy by the vibration energy harvester devices. When the energy translates from the vehicle to the bridge, the energy distributes over a very large structure. The energy absorbed by the vibrational energy harvester is therefore a very small fraction of the energy wasted by the vehicles. This is the first shortcoming of the traditional approach in bridge vibrational energy harvesting. The second disadvantage of conventional devices is that they will be useful only when installed on bridges. The vibrations of the regular portions of the roads are not sufficiently large to result in notable electrical energy.

The third drawback of bridge vibrational energy harvesters is their limited frequency bandwidth. This issue has received significant attention in recent years [8–15]. To overcome these challenges we propose a piezoelectric buckling harvester that directly converts the energy of passing vehicles or crowds to electricity. The piezoelectric beam oscillates freely in response to sudden changes of the load on the harvester. The energy harvester is therefore not resonant based and is insensitive to the frequency of the excitations.

A number of groups have studied energy harvesting of buckled piezoelectric beams. Buckling has been used in different contexts for energy harvesting. An axial load is most often used to affect the dynamics of the piezoelectric beams [16–20]. In these configurations, the ambient oscillations excite the beam laterally and the axial load or the axial displacement is constant. The axial load is directly used as a source of excitation in [21–24]. In this configuration, the successive buckling of the piezoelectric beam can result in a frequency up-conversion mechanism. In this method, however, the axial load is not constrained and its excess can easily damage the piezoelectric beam. In the presented energy harvester, not only do we use the load as an axial force excitation and thus generate significant amounts of power, but we also constrain the axial deformation to prevent fracture of the brittle piezoelectric beams.

In this paper, vertical and horizontal configurations of the piezoelectric buckling harvesters are investigated. A vertical piezoelectric beam is used to directly generate electricity using the load of the passing vehicles. Piezoelectric ceramics are brittle, and easily fracture when subjected to concentrated stresses. The piezoelectric patches are usually bounded to stiff materials such as metals or carbon fiber composites [25]. The buckling of a beam can result in large deformations of the beam, which may cause damage to the piezoelectric patch. In the proposed device, we make sure that the buckling of the beam is safe and will not cause damage. By using a mechanical safety stop, the amount of buckling of the beam is limited and controlled, so low-cycle fatigue will not be an issue in our device. In our design, the device is non-resonant and at the same time the power generated from piezoelectric beam is significant. The generated power can be in the order of tens of milliwatts. The proposed design is scalable and can be designed to fit in a shoe heel. This will make it possible to generate electricity with each step of a person. The power can be used for charging smart phones, players, or motion sensors [26], to make the wearable devices self-powered.

This paper proceeds by more detailed discussion of vertical and horizontal device configurations. Electromechanical models for vibration and energy harvesting characteristics of the device are presented. The models are numerically solved to predict the performance of the device. Finally, the effect of the length and thickness of the active layer on the generated power is discussed through a parametric study.

2. Device configuration

In this section, we discuss vertical (direct) and horizontal (indirect) device configurations of the energy harvester. In the vertical configuration the weight of the passing load is directly transmitted to the piezoelectric beam. The vertical beam consists of a steel layer as a substrate and two piezoelectric layers. The proposed device (figure 1) is installed on roads such that the vehicles directly pass over it. The transduction element that converts mechanical vibrations to electrical energy is the vertical piezoelectric bimorph. Three key objectives are sought in this design. The first objective is to have a robust energy harvesting device, i.e. to generate energy from every passing tire. The second objective is to maximize the amount of energy and to induce maximum amount of stress in the piezoelectric layer without breaking it. The third goal is to have a durable device. We should, therefore, limit the maximum stress in the piezoelectric layer to the allowable stress level for high-cycle fatigue. By implementing a mechanical stop we control the amount of buckling and prevent fracture of the piezoelectric beam due to excessive stresses.

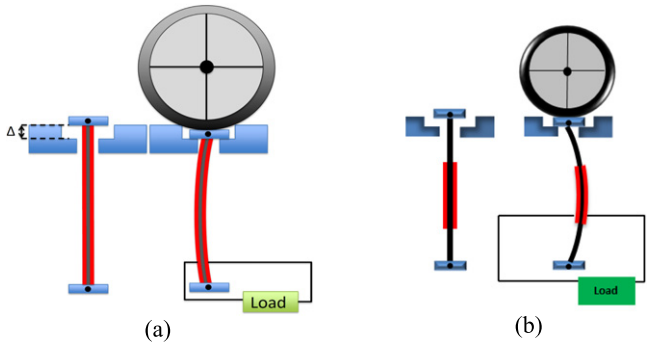

Figure 1. The vertical modeling of the energy harvesting device for a uniform beam (a) and a segmented beam (b).

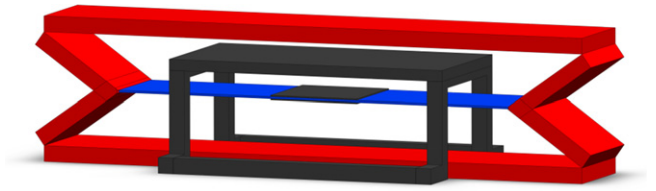

Figure 2. The horizontal (indirect) configuration.

Figure 1 shows the uniform and the segmented beam in the direct configuration. In our design, the larger the axial deformation of the beam, the easier the control of the stress in the piezoelectric patches. This axial deformation significantly increases with the length of the beam. An axial deformation in millimeters requires the length of the beam to be on the order of tens of centimetres. To increase the length of the beam without significantly increasing the cost, we need to cover only part of the beam with piezoceramics. The parts that are covered with piezoceramics are the parts of the beam that are under maximum bending stress. For a pin–pin beam, this part is the middle section of the beam. As is shown on figure 1(b), a non-uniform segmented beam consists of three different parts. The bottom (first) and top (third) sections of the beam are just a simple spring steel layer. The middle (second) section is a bimorph piezoelectric beam, with two active layers on the surfaces and one spring steel layer in between.

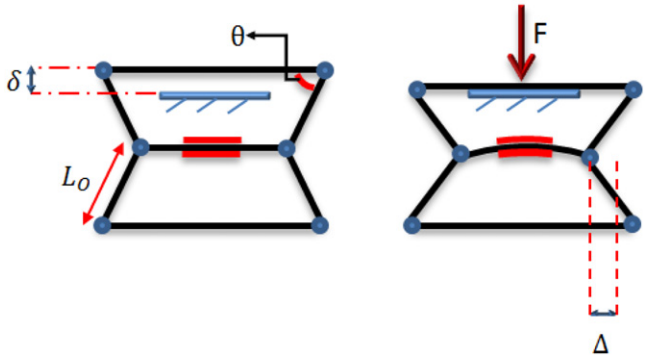

Figure 3. The horizontal energy harvesting device: undeformed (left) and after buckling (right).

The piezoelectric layer generates power when it buckles and when it returns to the undeformed shape. When the force is removed, the beam returns to its non-deformed position.

The horizontal (indirect) configuration is another type of energy harvester device studied in this paper. As illustrated in figure 2, the proposed device consists of a scissor linkage mechanism. The rigid scissor mechanism has two functions. Its first function is to convert the vertical load to a horizontal axial force across the piezoelectric segmented beam. The second role of the mechanism is to scale the axial deformation of the beam to a more prominent vertical displacement to make the buckling control easier.

The static governing equations are (figure 3):

$$P = F\cot(\theta),$$
$$\delta = \Delta\cot(\theta), \tag{1}$$

where F is the vertical force, P is the axial force acting on the piezoelectric beam, θ is the angle defined in figure 3, δ is the vertical gap distance, and Δ is the axial shortening of the segmented beam. As seen in equation (1) if the angle is less than 45°, P will be larger than F and the mechanism magnifies the vertical force. This configuration results in a large force on the active beam with just a very small force over the harvester F. This feature makes this harvester useful for portable devices and for applications in which the forces are small. The horizontal form factor of the device makes it easy to implement in sidewalks or shoe soles. Another advantage of having the angle less than 45° is the magnification of the gap distance δ. Since in this configuration δ is larger than Δ, the axial stop can be incorporated in the vertical direction to make the fabrication tolerances more relaxed. If the angle is more than 45°, P will be smaller than F, which makes this configuration suitable for installing on roads and under large forces. By increasing the angle, we make sure that the applied force on the segmented beam will not exceed the allowable amount and will not result in breaking the beam. In this paper we call the required gap size *the recess.*

3. Modeling and governing equations

The partial differential governing equations for the vibrations of the piezoelectric beam are derived through equilibrium method [8, 9, 27]. The mechanical governing equation for the covered portion of the beam is:

$$m\frac{\partial^2 w}{\partial t^2} + c\frac{\partial w}{\partial t} + EI\frac{\partial^4 w}{\partial x^4} + \left[P - \frac{K_{eq}}{2}\int_0^L \left(\frac{\partial w}{\partial x}\right)^2 \mathrm{d}x\right] \times \frac{\partial^2 w}{\partial x^2}\alpha\left[\frac{\mathrm{d}\delta(x)}{\mathrm{d}x} - \frac{\mathrm{d}\delta(x-L)}{\mathrm{d}x}\right]V(t) = 0, \tag{2}$$

where m is the total mass per unit length of the beam, $w(x, t)$ is the lateral deflection of the beam, EI is the equivalent bending stiffness of the composite beam, K_{eq} is the equivalent stiffness of the active beam, α is the piezoelectric coupling coefficient, and V is the voltage across the piezoelectric elements that are connected in parallel. The width of the beam is denoted by b, the thickness of the substrate is t_s, and the thickness of the piezoelectric layer is t_p. $\delta(x)$ is the Dirac delta function. The coupling term, α, for the parallel connection can be written as [28]:

$$-2\int_{\frac{t_s}{2}}^{t_p+\frac{t_s}{2}} e_{13}\frac{b}{t_p}z\mathrm{d}z = -2be_{13}\frac{t_p + t_s}{2}, \tag{3}$$

where e_{13} is the piezoelectric coefficient. If the axial force is larger than the critical buckling force, the beam buckles. In this paper, we assume that the force is larger than the first critical load and is less than the critical load of the higher modes. We therefore, only consider the first buckling mode shape for discretization of the governing equations. We assume that the buckling mode shapes are identical to the vibration mode shapes of the beam. To derive the natural frequencies and mode shapes of the segmented beam, we first write the undamped unforced governing equations for each segment:

$$\rho A\frac{\partial^2 w}{\partial t^2} + EI\frac{\partial^4 w}{\partial x^4} = 0. \tag{4}$$

We will use modal analysis to discretize the equations of motion (section 11 of [29]):

$$\mathrm{w}(x, t) = \sum_{j=1}^{\infty}\phi_j(x)T_j(t), \tag{5}$$

where, ϕ_j is the jth mode shape and T_j is the corresponding temporal function. Substituting equation (5) in equation (4) , the general solution for a segmented beam can be found in the form of:

$$\phi_{ji}(x) = a_{ji1}\sin\left(\frac{\beta_j}{\sqrt{C_i}}x\right) + a_{ji2}\cos\left(\frac{\beta_j}{\sqrt{C_i}}x\right) + a_{ji3}\sinh\left(\frac{\beta_j}{\sqrt{C_i}}x\right) + a_{ji4}\cosh\left(\frac{\beta_j}{\sqrt{C_i}}x\right), \tag{6}$$

where i is the ith beam section and j shows the jth mode shape. a_{ji1}, a_{ji2}, a_{ji3}, a_{ji4} and β_j are calculated from the

boundary conditions. and C_i is [29, 30]:

$$C_i = \sqrt{\frac{E_i I_i}{\rho_i A_i}} \ . \tag{7}$$

If the beam is entirely covered with piezoelectric material, it represents a uniform simply supported beam, and the mode shapes are [29]:

$$\phi_j(x) = A \sin\left(j\frac{\pi x}{L}\right). \tag{8}$$

The mode shapes of a segmented beam are different from those of a uniform beam. Each mode shape is a three-part function where each function quantifies the mode shape over a segment of the segmented beam. The beam has three segments and the deflection shapes are different for each part. The mode shape functions over each segment of the beam are represented by equation (6). So, there are, in total, 12 unknown coefficients (a_{j11}, a_{j12}, …, a_{j34}). There are four boundary conditions at the two ends. (The deflection (ϕ) and bending moment ($EI\phi''$) are zero.) Because of continuity and equilibrium conditions, we have four conditions at each of the interfaces. In other words, at these points, the two sides should have the same deflection, slope, shear force, and bending moment. Four boundary conditions at the two ends and eight equilibrium and continuity equations at the two interfaces give the 12 equations to solve for the 12 unknowns:

$$\begin{cases} \phi_{j1}(0) = 0 \\ \phi_{j3}(l_1 + l_2 + l_3) = 0 \\ \phi''_{j1}(0) = 0 \\ \phi''_{j3}(l_1 + l_2 + l_3) = 0 \\ \phi_{j1}(l_1) = \phi_{j2}(l_1) \\ \phi'_{j1}(l_1) = \phi'_{j2}(l_1) \\ E_1 I_1 \phi''_{j1}(l_1) = E_2 I_2 \phi''_{j2}(l_1) \\ E_1 I_1 \phi^{(3)}_{j1}(l_1) = E_2 I_2 \phi^{(3)}_{j2}(l_1) \\ \phi_{j2}(l_1 + l_2) = \phi_{j3}(l_1 + l_2) \\ \phi'_{j2}(l_1 + l_2) = \phi'_{j3}(l_1 + l_2) \\ E_2 I_2 \phi''_{j2}(l_1 + l_2) = E_3 I_3 \phi''_{j3}(l_1 + l_2) \\ E_2 I_2 \phi^{(3)}_{j2}(l_1 + l_2) = E_3 I_3 \phi^{(3)}_{j3}(l_1 + l_2) \ . \end{cases} \tag{9}$$

ϕ_{j1} is the deflection of the first part, ϕ_{j2} is the deflection of the middle section of the beam, and ϕ_{j3} is the deflection of the third part of the beam. ϕ'_{ji} represents the slope in each part, $E_i I_i \phi''_{ji}$ is the bending moment of the beam, and $E_i I_i \phi^{(3)}_{ji}$ is the shear force of the beam. To find the unknown coefficients we write the 12 equations in (9) and write them in the matrix form: $BA = 0$. B is a 12 × 12 matrix and A is defined as:

$$\mathrm{A} = [a_{j11}\ a_{j12}\ \ a_{j13}\ \ a_{j14}\ \ a_{j21}\ a_{j22}\ \ a_{j23}\ a_{j24}\ a_{j31}\ a_{j32}\ a_{j33}\ \ a_{j34}]^T. \tag{10}$$

Non-trivial solutions only exist if the determinant of matrix B is zero. In order to find the β that makes the determinant zero, we plot the logarithm of the determinant of matrix B in terms of different βs. The first drop in the plot is associated with the frequency of the first mode shape, the second drop in the plot is the frequency of the second mode shapes, and the next drops are associated with the next natural frequencies. To find the exact frequency, we use the Newton–Raphson method using the estimated frequencies from the aforementioned plot as the initial guess. In this paper, we consider just the first two frequencies in order to find the first two mode shapes and their critical buckling force.

If the determinant of B matrix is zero, there is not a unique answer for the set of equations. So in order to solve them, one equation should be eliminated. Next, a value for one of the components of the vector A is assumed, and the other 11 remaining coefficients are derived based on that component. We need to check to see if the choice of the arbitrary component has been proper. In some cases that assumed component in the coefficient vector is zero. This means that, our first assumption is not correct, and we need to take another element as the assumed component. In order to check to see if the assumption is correct, we remove the column and the row associated with that assumed coefficient from matrix B, and check the rank of the remaining square matrix. If the rank is $n - 1$ (11 in this case), our assumption was correct and we can proceed. But if the rank is less than $n - 1$, we remove another row instead of the one, which was removed. A more numerically efficient method for derivation of the natural frequencies and the mode shape is presented in the appendix.

In our calculation we use the mass normalized mode shapes [31]:

$$\int_0^L \phi_{ij}(x) m_i \phi_{ij}(x) \mathrm{d}x = 1 \ . \tag{11}$$

Figure 4 compares the deformation shape of a segmented deflected beam under axial force and that of a uniform beam. For validation of our method, we consider a special case: we assume that the thickness of the piezoelectric layer in the middle section is zero. As expected, the deflection shape is identical to that of a uniform beam. The critical buckling force is checked for both cases and it is the same in both cases.

After finding the deflection of the beam we replace $w(x, t)$ with $w(x, t) = \sum_{j=1}^{\infty} \phi_j(x) T_j(t)$ in equation (2) and we pre-multiply the equation by the mode shape. If we integrate the expression from zero to the length of the beam,

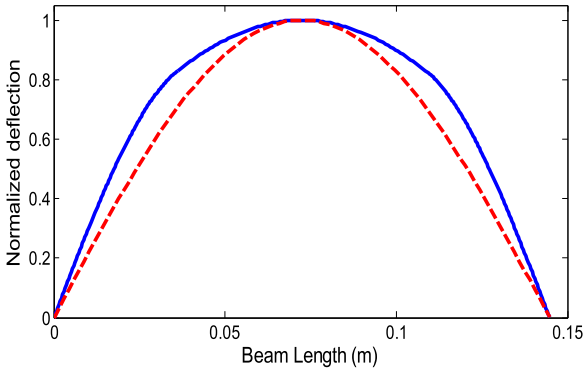

Figure 4. Deflection of uniform beam (dashed line) versus segmented beam with two piezoelectric layers in the middle.

we get:

$$m\int_0^L \phi_k\, dx\sum_{j=1}^{\infty}\phi_j(x)\ddot{T}_j(t) + c\int_0^L \phi_k dx\sum_{j=1}^{\infty}\phi_j(x)\dot{T}_j(t) + EI\int_0^L \phi_k dx\sum_{j=1}^{\infty}\phi^{(4)}{}_j(x)T_j(t) + \int_0^L \phi_k dx\left[P - \frac{K_{eq}}{2}\times\int_0^L\sum_{j=1}^{\infty}\phi'^2{}_j(x)T_j(t)dx\right]\sum_{j=1}^{\infty}\phi''{}_j(x)T_j(t) + \alpha\int_0^L \phi_k dx\left[\frac{d\delta(x)}{dx} - \frac{d\delta(x-L)}{dx}\right]V(t) = 0. \quad (12)$$

Due to orthogonality of the mode shapes the modal equations are decoupled:

$$M_k\ddot{T} + c\dot{T} + \left(K_k - p_k\right)T + N_kT^3 + \beta_k V(t) = 0, \quad (13)$$

where M_k is the modal mass of the kth mode, c is the damping ration, K stands for the linear stiffness, p is the reduction of the stiffness coefficient due to the axial force, N is the nonlinear coefficient, and the coupling coefficient is β. These integrals were calculated analytically for a uniform beam:

$$\begin{cases} M = m\int_0^L \phi^2(x)dx = \dfrac{mA^2L}{2}, \\ K = EI\int_0^L \phi^{(4)}(x)\phi(x)dx = A^2EI\,\dfrac{\pi^4}{2L^3}, \\ p = -P\int_0^L \phi''(x)\phi(x)dx = A^2P\,\dfrac{\pi^2}{2L}, \\ N = -\dfrac{K_{eq}}{2}\int_0^L \phi'^2(x)dx\int_0^L \phi''(x)\phi(x)\,dx \\ \quad = A^4EA\,\dfrac{\pi^4}{8L^3}, \\ \beta = \alpha[\phi'(L) - \phi'(0)] = -2\alpha A\dfrac{\pi}{L}. \end{cases} \quad (14)$$

For a segmented beam, the integrals in equation (14) were calculated numerically. The critical buckling force of the beam is the amount of axial force, P, that makes p equal to K.

Figure 5 shows the equivalent electrical circuit for the energy harvester. The governing equation using Kirchhoff's law is [32]:

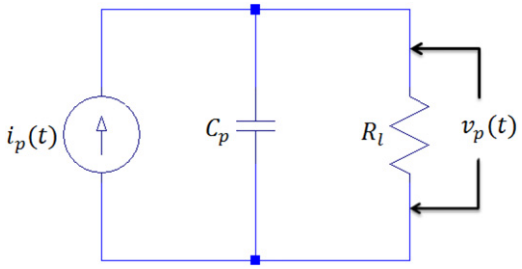

Figure 5. Electrical circuits for the harvester.

$$C_p\,\dot{V} + \frac{V}{R_l} = \beta\dot{T}, \quad (15)$$

where R_l is load resistance, and the capacitance of the piezoelectric is $C_p = n\,\epsilon_0\frac{Lb}{t_p}$, in which n is the number of piezoelectric layers (two in our device). The governing equations before the stop is engaged are:

$$\begin{cases} M\ddot{T} + c\dot{T} + (K-p)T + NT^3 + \beta V(t) = 0, \\ C_p\dot{V} + \dfrac{V}{R_l} = \beta\dot{T}. \end{cases} \quad (16)$$

If the axial force is less than the critical load, the zero deflection equilibrium would be stable. However, if the axial force surpasses the first critical load, the zero deflection equilibrium becomes unstable. In that situation, due to the existence of the nonlinearities, another stable equilibrium exists. The modal coordinate representing the nonlinear equilibrium point is:

$$T^2 = \frac{(p-K)}{N}. \quad (17)$$

The governing differential equations in equation (2) are valid before the stop is engaged. When the support is engaged, the external load is applied to the support and equation (16) is not valid. In that situation the axial displacement of the beam is fixed at the designed recess (figure 1). In this situation, the problem changes from a fixed axial force problem to a fixed axial displacement problem. The governing equations for the vibration of an axially displaced beam is presented in [33] as:

$$m\frac{\partial^2 w}{\partial t^2} + c\frac{\partial w}{\partial t} + EI\frac{\partial^4 w}{\partial x^4} + \left[K_{eq}\Delta - \frac{K_{eq}}{2}\int_0^L\left(\frac{\partial w}{\partial x}\right)^2 dx\right]\frac{\partial^2 w}{\partial x^2} = 0. \quad (18)$$

The model manifested in equation (18) implies that the effect of an axial fixed displacement of Δ is equal to the effect of an axial force of $K_{eq}\Delta$. Unfortunately this model does not seem to be correct. The first incorrect result of equation (18) is on the static axial deformation of the beam. In static situation the axial deformation of the beam must be equal to Δ. The

axial deformation of the beam is given by

$$d = \int_0^L \frac{1}{2}\left(\frac{\partial w}{\partial x}\right)^2 \mathrm{d}x.$$

For a uniform beam the axial deformation resulted from this equation and equation (18) is $d = \Delta - \frac{AL}{I\pi^2}$. This contradicts the boundary conditions. We suggest that the correct equivalent axial force should be $K_{\mathrm{eq}}\Delta + p_{\mathrm{c}} = K_{\mathrm{eq}}\Delta + \frac{EI\pi^2}{L^2}$ where p_{c} is the critical load. This value is consistent with $d = \Delta$. The difference between the two values becomes obvious in the following thought experiment. Assume that the deformed axial length of the beam is a slight amount (ε) shorter than L. Since the shortening of the neutral axis is negligible, the beam has to buckle to accommodate to the boundary conditions. The equivalent axial force should therefore be larger than the critical buckling load. This condition is satisfied by our corrected equivalent load but is contradicted with the expression in [33]. So, we suggest that the correct formula is:

$$m\frac{\partial^2 w}{\partial t^2} + c\frac{\partial w}{\partial t} + EI\frac{\partial^4 w}{\partial x^4} + \left[K_{\mathrm{eq}}\Delta + p_{\mathrm{c}} - \frac{K_{\mathrm{eq}}}{2}\int_0^L \left(\frac{\partial w}{\partial x}\right)^2 \mathrm{d}x\right]\frac{\partial^2 w}{\partial x^2} = 0. \quad (19)$$

Thus, after the stop is engaged, instead of equation (16) the governing equations are [34]:

$$\begin{cases} M\ddot{T} + c\dot{T} + \left(K - p_{\mathrm{e}}\right)T + NT^3 + \beta V(t) = 0, \\ C_{\mathrm{p}}\dot{V} + \dfrac{V}{R_l} = \beta\dot{T}. \end{cases} \quad (20)$$

The parameters definitions are similar to those in equation (16). The only difference is the reduction of the stiffness coefficient due to the axial force:

$$p_{\mathrm{e}} = -\left(P_{\mathrm{stp}} + P_{\mathrm{c}}\right)\int_0^L \phi''(x)\phi(x)\mathrm{d}x. \quad (21)$$

In this equation P_{c} is the first critical load for buckling and P_{stp} the equivalent axial force in equation (19) which is equal to $P_{\mathrm{stp}} = K_{\mathrm{eq}}\Delta$. Where Δ is the shortening in the beam when the stop is hit and K_{eq} is the equivalent stiffness of the segmented beam: $\frac{1}{K_{\mathrm{eq}}} = \frac{L_1}{E_1A_1} + \frac{L_2}{E_2A_2} + \frac{L_3}{E_3A_3}$.

The critical force for buckling is defined as the amount of force that makes the linear part of equation (16) zero ($p = K$). So, the critical force is:

$$P_{\mathrm{c}} = \frac{\int_0^L \phi''(x)\phi(x)\mathrm{d}x}{EI\int_0^L \phi^{(4)}(x)\phi(x)\mathrm{d}x}. \quad (22)$$

For a uniform beam the value of p_{e} and p_{c} are equal to:

$$p_{\mathrm{e}} = A^2\left(\frac{EA}{L}\Delta + p_c\right)\frac{\pi^2}{2L},\ P_{\mathrm{c}} = EI\frac{\pi^2 n^2}{L^2}, \quad (23)$$

where n is the number of the buckling mode. For the vertical configuration, the maximum shortening of the beam is equal to the gap between the device and the support (Δ). For the indirect configuration, equation (1) relates the shortening of the beam and the required gap size.

4. Design

The purpose of the stop is to prevent fracture of the beam under buckling deformations. This is achieved by limiting the amount of axial deformation of the beam. In this section, we calculate the safe gap size for uniform and segmented beams. First, we calculate the amount of axial deformation of the beam, which corresponds to maximum allowable stress in the materials. Based on the equation for the shortening of the beam, the amount of maximum shortening of the beam ($\Delta_{\max}$) is proportional to the second power of the maximum allowable strain in the beam:

$$\Delta_{\max} \propto \epsilon_{\max}^2. \quad (24)$$

The allowable strain is related to the allowable stress as:

$$\epsilon_{\max\,\mathrm{s}} = \frac{\sigma_{\mathrm{ys}}}{E_{\mathrm{s}}},\quad \epsilon_{\max\,\mathrm{p}} = \frac{\sigma_{\mathrm{yp}}}{E_{\mathrm{p}}}, \quad (25)$$

where $\epsilon_{\max\,\mathrm{s}}$ and $\epsilon_{\max\,\mathrm{p}}$ are the maximum allowable strain in the substrate and piezoelectric patches. σ_{yp} and σ_{ys} are the yield stress for the substrate and piezoelectric layers. E_{p} and E_{s} are the module of elasticity for the piezoelectric material and the substrate. In segmented beams the relation between $\epsilon_{\max}$ and $\Delta_{\max}$ is more complicated than that of the uniform beams. The first complication is that the fracture can occur at the piezoelectric patch or at the substrate. In the covered sections, the fracture occurs at the piezoelectric patch. The fracture of the non-covered sections naturally occurs due to the fracture of the substrate. We first calculate the strains occurring over the piezoelectric material and the substrate for an arbitrary beam deformation. We will then identify the most susceptible part of the beam and will calculate the axial deformation which causes the fracture of the beam at its most susceptible point. The considered arbitrary deformation is that corresponding to a modal coordinate of one. The procedure is to first find this axial deformation. We also find the maximum strain over all the length of the beam at this modal deformation. We will then locate the most susceptible fracture point, and compare the value of the calculated strain to the maximum allowable strain at that point. Since the axial deformation is proportional to the second power of the strain, a scaling factor can be calculated to give the beam axial shortening corresponding to the maximum allowable strain. This beam allowable shortening identifies the recess in this design.

The axial deformation corresponding to the modal coordinate of one is Δ_0, the maximum strain of the piezoelectric patch is $\epsilon_{0\mathrm{p}}$, and the maximum strain of the

substrate is ϵ_{0s}:

$$\Delta_0 = \int_0^L \frac{1}{2}\left(\frac{\partial w}{\partial x}\right)^2 \mathrm{d}x,$$
$$\epsilon_{0p} = \left(t_p + \frac{t_s}{2}\right)\cdot \mathrm{Max}\left[\phi_2''(x)\right],$$
$$\epsilon_{0s} = \left(\frac{t_s}{2}\right)\cdot \mathrm{Max}\left[\phi_1''(x)\right]. \quad (26)$$

For a uniform beam the maximum strain occurs at the middle of the beam. This is not necessarily the case in segmented beams since the most susceptible point can be on the covered patch or the uncovered regions. In the next step, based on equations (24) and (26) we can find the maximum allowable shortening in the beam (Δ_{max}). In order to find Δ_{max} we calculate this value both for substrate ($\Delta_{s,max}$) and the piezoelectric layer ($\Delta_{p,max}$):

$$\Delta_{s,\,max} = \left(\frac{\epsilon_{s,\,max}{}^2}{\epsilon_{0s}{}^2}\right)\Delta_0, \quad \Delta_{p,\,max} = \left(\frac{\epsilon_{p.max}{}^2}{\epsilon_{0p}{}^2}\right)\Delta_0. \quad (27)$$

The Δ_{max} is set to the smaller number between $\Delta_{s,max}$ and $\Delta_{p,max}$. The other thing we should notice in designing the device is that the system is designed to have low damping coefficient to enhance the power generation. As a result, the beam might deform more than expected from static analysis of the buckling of the beam. So, a safety factor is considered for the gap size in the final stage.

The solution is divided into different parts. The first part is when the force is over the device and the beam moves down until it hits the support. In this part, equation (2) is the governing equation for the vibration of the piezoelectric beam. After the beam buckles the support is engaged, equation (19) is the governing equation of the system. When the force is removed, the piezoelectric beam tends to spring back and equation (2) gives the solution of the system. Since there is no force over the harvester in this situation, p equals zero in the equation. Since both equations (2) and (19) are nonlinear, we use numerical integrations to solve the model and predict the power generated by the energy harvesting device.

To design the energy harvesting device, we need to make sure that the stresses in neither piezoelectric layer nor the substrate exceed the corresponding yield stress. If the force exceeds the limit, the stress will break the harvester. The horizontal configuration could be implemented in shoe soles or sidewalks, using loads of passing crowds over the harvester. So, the amount of force we expect on the upper beam is about human weight. Since this force would become larger in the case of jumping or running over the device, we consider a safety factor in our design. The vertical configuration could be implemented in the roadways, generating electricity using the force of the passing cars. We consider a safety factor to make sure the device does not break under the weight of heavier vehicles. The next step is to check if the weight is more than the first critical buckling load of the piezoelectric beam. In order to calculate the first critical buckling force, the first vibration mode shape is considered as $\phi(x)$ in the equation (23). Similarly, for calculating the nth buckling critical force, $\phi(x)$ in equation (23) is replaced by the nth mode shape. Since there usually is some level of charge cancellation associated with the higher modes [35], we only utilize the first buckling mode shape in our design. Thus, the force over the piezoelectric beam has to be more than the first critical buckling load and less than the second critical buckling load. First and second critical buckling forces are shown for different thicknesses and lengths of piezoelectric layers in figure 6. For a uniform simply supported beam, the critical buckling force is calculated using equation (23). As the equation shows, the second critical buckling force in a uniform beam is four times the first critical buckling force. The interesting result about the segmented beam is that the ratio of the second to the first critical buckling force changes with the length and thickness of the middle part. Figure 6 shows the first and second critical buckling force for a segmented beam in vertical configuration. As the length of the middle part decreases, both critical forces increase, and so does the ratio of the second critical force to the first. For our design the desired force over the segmented beam should stay between these two surfaces shown in the plot.

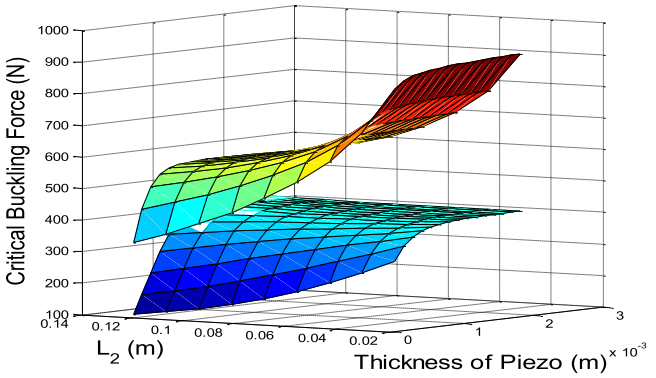

Figure 6. First critical buckling force (lower surface) versus second critical buckling force as a function of thickness of the piezoelectric layer and the length of the middle part.

5. Results

In this section we study three different case studies. The first study involves a uniform beam in the vertical configuration. The second case is the vertical configuration with a segmented beam. In both cases the force over the device is considered to be the weight of a car. The last case study is a segmented beam in the horizontal configuration. The indirect device is designed to generate electricity from human weight. The output power and the gap size are calculated for all three cases and ultimately the effect of design parameters on the output power and gap size is studied.

5.1. Uniform beam

We investigate a case study for the direct configuration, using the uniform beam (figure 7). A 10 inch (254 mm) long and 1.5 inch (38.1 mm) wide piezoelectric bimorph with 0.03 inch

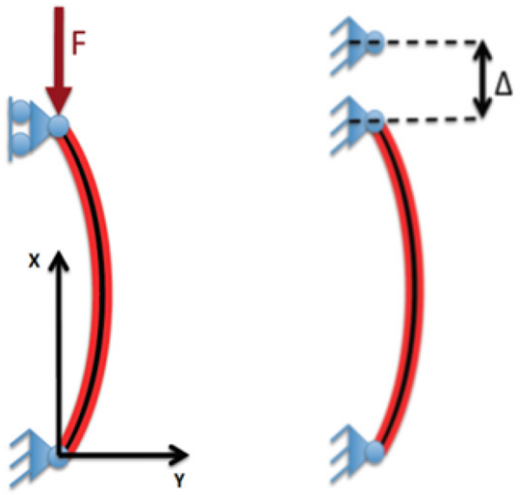

Figure 7. Schematic of a uniform beam in the buckled position.

(762 μm) thick steel substrate and 0.04 inch (1016 μm) PZT-5A piezoelectric patches meets all the requirements mentioned in the design section to be used as the bending element in the vibrational energy harvester. PSI-5A4E Piezo sheets from Piezo Systems, Inc. are used as the piezoelectric layer.

Figure 8(a) shows the dimensionless deflection of the beam, which is the temporal term in modal expansion (T) divided by the temporal term that results in maximum allowable stress ($T_{\max}$). When the dimensionless deflection is equal to one, the beam is at the border of fracture. One fourth of the weight of a car, which is the force on each tire, is considered as the axial force over the device (2450 N). If the axial force increases, the amplitude of the free oscillations increases and the height of the peaks in figure 8(a) will be larger. This increases the amount of output power. Therefore the best power output is achieved if there is a quickly repeating large force over the harvester. It is also interesting that after the engagement of the safety stop, the beam continues to oscillate. In other words, the motion of the beam is completely dynamic and oscillatory at almost every moment. The piezoelectric beam performs free oscillations after each sudden change of the axial force. Since the free oscillations are at the natural frequency of the harvester the power generation frequency is at the optimal value. The free vibration nature of the energy harvesting element implies that the *energy* generated from each sudden force variation is fixed. Thus, the more frequent the variations of the axial load, the more *power* is generated.

The instantaneous power across a 10 kΩ resistive load is plotted in figure 8(b). The value of the resistive load is selected to match the impedance of the piezoelectric layer when the beam oscillates under no axial force at its fundamental natural frequency (equation (28)). The average power for generated electricity in figure 8(b) is 42.3 mW. The gap distance is 0.02 mm.

5.2. Segmented beam

Next, we study both configurations using the segmented beam instead of the uniform beam. For the direct configuration, PSI-5A4E Piezo sheets from Piezo Systems, Inc. are considered as the piezoelectric element. We use a piezoelectric bimorph beam for the middle part with a 101.6 mm long and 38.1 mm wide with 1778 μm thick steel substrate and 508 μm thick PSI-5A4E (the piezoelectric material) piezoelectric patches. The lengths of the first and third parts of the beam are 76.2 mm. Figure 9(a) illustrates the dimensionless deflection of the beam and figure 9(b) shows the instantaneous power across an 8 kΩ resistive load (the value of the shunt resistance is chosen to match the impedance of the piezoelectric element at the first natural frequency). Quarter weight of a typical car (2450 N) is the applied axial force on the device.

As illustrated in the figure 9(a), the majority of the electricity is generated after the force is removed. To study the relation between the load resistance and the generated power, the average power $\left(\frac{{V_{\rm rms}}^2}{R}\right)$ for different resistances were calculated. It is shown in figure 10 that when resistance equals 8 kΩ, we have the maximum generated power. This resistance is close to the resistance calculated as:

$$R = \frac{1}{C\,\omega}, \tag{28}$$

where C is the capacity of the piezoelectric layer and ω is the natural frequency of the beam. The value calculated from equation (28) is 10 597 Ω. The duration of force being applied to the harvester is assumed to be 0.05 s. After the force is removed the beam springs back. The average power for generated electricity in figure 9(b) is 27.3 mW. The gap distance is 0.035 mm.

For the indirect configuration (figure 2), we use a piezoelectric bimorph beam for the middle part with a 76.2 mm long and 72.4 mm wide with 2032 μm thick steel substrate and 2032 μm thick piezoelectric patches (PSI-5A4E from Piezo Systems, Inc.). By using this beam in our device we make sure that the applied force is more than the first critical load of the piezoelectric beam and also less than the second critical load. The lengths of the first and third parts of the piezoelectric beam are 127 mm. The length of the oblique beams (L_0 in figure 3) is 3 inches and the angle between the upper beam and oblique beams (θ in figure 3) is 10°. With this angle, we make sure that there is sufficient force for buckling of the beam (for this case the first critical buckling force is 1458 N). If we decrease the angle, the force needed for buckling the device would decrease, but having a very small θ angle makes the building of the device impractical. The calculated safety factor for the axial load is 15 and 8 for the substrate and piezoelectric layers (the yield stress is assumed 40 MPa and 250 MPa for these layers). Since the motion of the beam is oscillatory even after the stop is hit, another safety factor is considered in the last step of the design. The main advantage of indirect configuration over the vertical configuration is the increase in the safety recess. The required gap size is maximum allowable shortening of the beam ($\Delta_{\max}$) multiplied by the cotangent of θ. If θ is less than 45°, the required gap size is larger than $\Delta_{\max}$. A larger gap would make the building and implementing of the device more convenient.

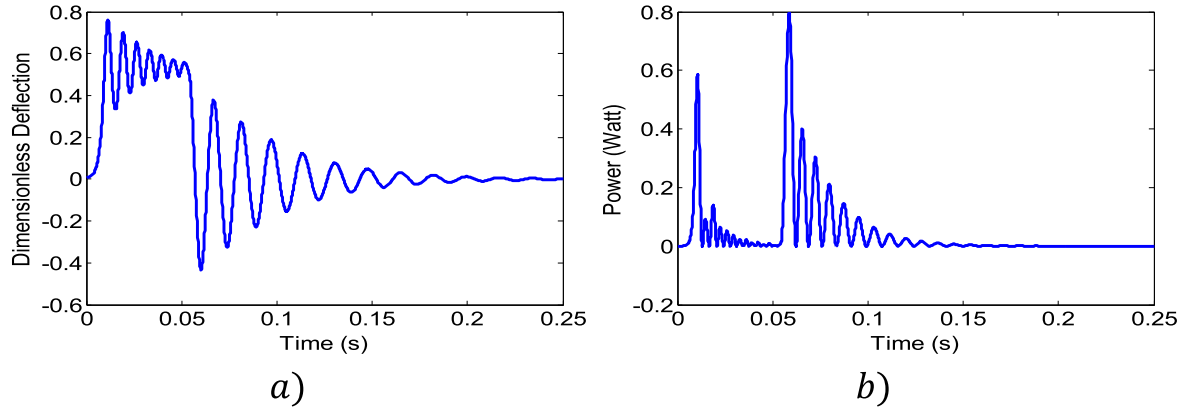

Figure 8. (a) Dimensionless displacement and (b) instantaneous power of a uniform beam in the direct configuration.

Figure 11(a) shows the dimensionless displacement of the segmented beam in the horizontal device. The duration of the load is assumed 0.2 s. Since the force over the horizontal device is assumed to be human weight, the force duration is larger than that of the vertical case. The beam springs back to the zero equilibrium position similar to the vertical configuration. The average power generated is 8.5 mW. Considering the fact that we used human weight for generating electricity in the harvester, the generated power is notable. Figure 12 shows the average power using different resistances. The maximum power is generated using a 42 kΩ resistive load (figure 11(b)). If we use equation (28), the resistive load is 26 kΩ, which is slightly different from the optimized resistance. Although these two resistive loads are different, the generated power does not change significantly if we use one of the resistances over the other one. The difference can be justified by the fact that the frequencies of the oscillations of the buckled and unbuckled beams are different. This difference in oscillation frequency translates to the difference in optimal shunt resistance. The same geometry can be used in a stress ball shaped energy harvester used for charging portable electronic devices.

The most important advantage of using a segmented beam over uniform beam is the increase in the required gap distance. The required gap is even larger in the horizontal configuration due to the usage of the linkage mechanism. The gap distance for the case study of the horizontal device is 0.8 mm, which is larger than vertical configuration and about forty times larger than uniform beam.

5.3. Design parameters

In this section, we study the effect of the design parameters on the power output and the gap size. In the horizontal configuration, the required gap decreases with θ. It is then desirable to consider small θ angles. One should observe the fabrication limitations in choosing the value of θ. The length of the lateral beam does not affect the recess significantly (figure 13(a)). So it could be concluded that the most important parameter design of a horizontal harvester is the θ angle.

The effect of the length of the piezoelectric layer and its thickness in the horizontal device is also illustrated in figure 13(b). As is shown in the figure, δ (recess gap) increases as the length of the piezoelectric layer (the middle part of the beam) increases. By increasing the thickness of the piezoelectric layer, at first the gap distance increases, but after a point it decreases because the piezoelectric layer is not the susceptible part of the piezoelectric beam. For thin piezoelectric layers, the substrate breaks before the piezoelectric layer, so it is crucial to ensure the safety of both piezoelectric layer and substrate. The deflection shape for a beam with a thick piezoelectric patch and a thin steel substrate is illustrated in figure 14. Because the beam is much thicker in the middle, it is more prone to damage at the interfaces of the middle segment and the other segments of the beam.

The relation between the thickness of the active layer (piezoelectric layer) and the length of the middle part of the beam and the output power for the indirect device is illustrated in figure 15. By increasing the length of the middle segment, the generated power of the device increases. As the overall length of the beam increases, the total stiffness of the beam decreases, which results in more vibration of the beam. The power output is directly related to the vibrations. Increasing the thickness of the piezoelectric layer to a certain extent can enhance the output power of the beam. Beyond that, the piezoelectric patch acts rigid and only the uncovered portions of the beam vibrate. As a result the generated power decreases.

6. Conclusion

In this paper, generation of electricity from uniform and segmented piezoelectric beams was studied. The mode shapes of the segmented beam were calculated and the electromechanical equations were solved for vertical and horizontal configurations. The load over the harvester results in buckling of the piezoelectric beam. This transition results in oscillations of the piezoelectric beam and causes power generation. After the force is removed (the person takes another step or the car passes over) the beam springs back to the unbuckled shape and more power is generated. To prevent the beam from fracture or damage, a mechanical stop is placed to limit the beam deformations. The direct design can be implemented in roads, using the weight of the passing cars to generate electricity. By using the segmented beam instead of a uniform

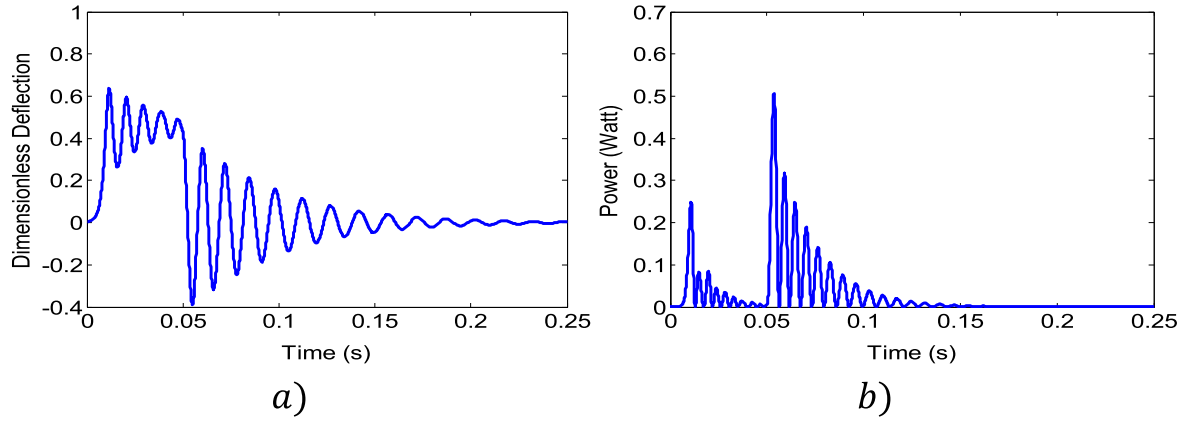

Figure 9. (a) Dimensionless displacement and (b) instantaneous power of a segmented beam in the direct configuration.

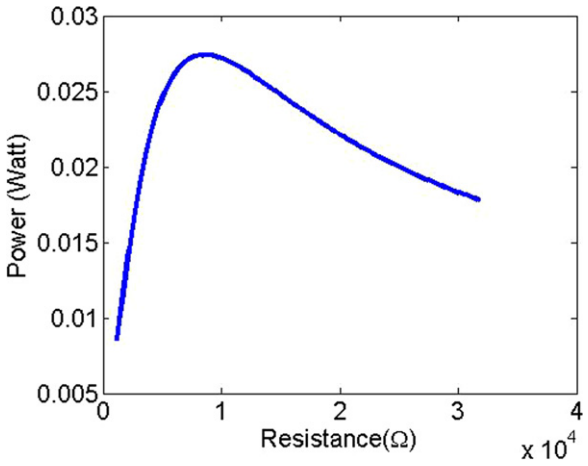

Figure 10. Average output power versus resistance for a segmented beam in the direct configuration.

beam the required gap distance increases, which makes this design more practical in terms of manufacturing. The force capacity of the indirect design is smaller than that of the direct design. This makes the direct design more suitable for energy generation from cars while the indirect design is more pertinent to power generation from human power. The indirect configuration makes it easy to implement in treadmills, shopping center floors, or dance floors and also makes it possible to use the human body weight as the source of applying force to the device and generating electricity. The required gap distance is also larger for the segmented configuration. It was shown that the gap distance of the horizontal design is about forty times than that of the vertical configuration. The required gap distances for different θ angles and different lateral beams were discussed and it was shown that θ angle is a critical parameter in designing the horizontal device. Governing equations of the system were derived for two vibration regimes (before engagement of the stop and after the engagement). The transient vibrations of the beam have been analytically modeled. The geometric nonlinearities of the beam have been taken into account. The deflection and output power of the device were calculated and studied for two case studies. The uniform direct design with a 254 mm long and 38.1 mm wide piezoelectric beam generates 42.3 mW and the required gap distance (Δ) is 0.02 mm. The load over the direct design is 2450 N. By using a segmented beam the required gap size increase to 0.035 mm. If we use a segmented beam in the indirect design, Δ increases to 0.8 mm and it generates 8.5 mW power. It was shown that there is an optimized resistance for each design that generates the maximum average power output. Finally, the effect of the length and thickness of the piezoelectric layers on the output power and also the gap distance were investigated.

Appendix

A more advanced way to find the coefficient is to reduce the 12×12 matrix using transformation matrices. The aim of this method is to reduce the size of the coefficient matrix to reduce the computational time and numerical errors [36]. The principle of this method, which we call the *transformation matrices method*, is to use the equilibrium and continuity conditions to transform the two boundary condition equations of one end of the beam to two equations for the other end. By having these two new equations, there are in total four equations for one end of the beam and we can find the natural frequencies of the system and four unknown coefficients of that end. By using this method we should calculate the determinant of a 4×4 matrix instead of a 12×12 matrix for the segmented beam case. This method would show a significant difference in calculation time when we have large matrices [36]. Although in our case the first matrix (12×12) is not very large, due to the high number of numerical calculations for the optimization of the device, we use the transformation matrices method. This method is very useful and time saving when it comes to the optimization part. In order to find the optimized thickness or length of the beam, we need new numerical calculations for every configuration. Considering the number of different configurations, using this method reduces the overall time of the calculations significantly.

We have two boundary conditions at each end of the beam; this results in four boundary conditions. Considering these

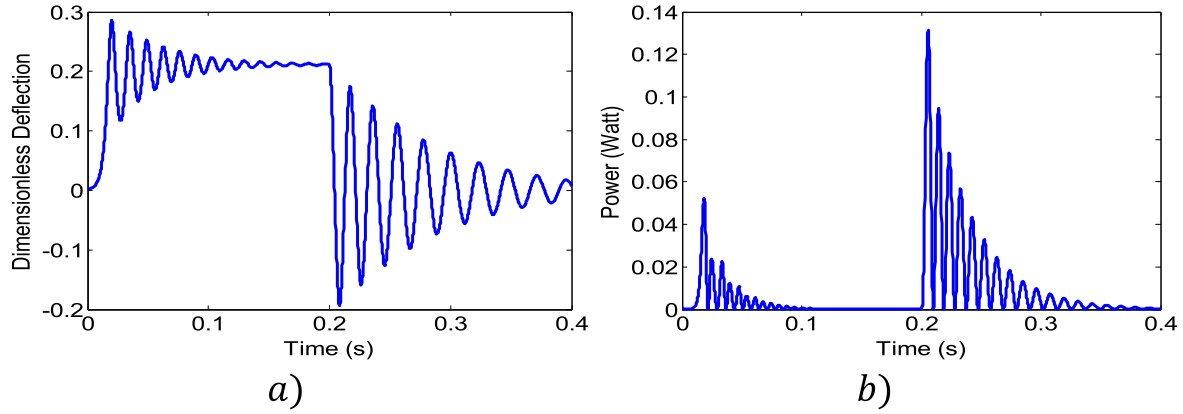

Figure 11. (a) Dimensionless displacement and (b) instantaneous power of a segmented beam in the indirect configuration.

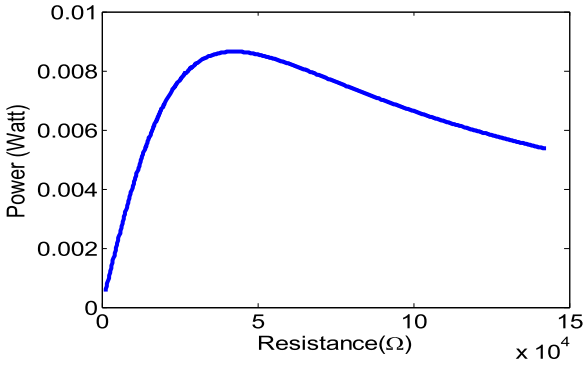

Figure 12. Average output power versus different resistances for a segmented beam in the indirect configuration.

boundary conditions at the two ends of the beam we have:

$$[B_{C0}]_{2\times4}\begin{bmatrix}a_{j11}\\a_{j12}\\a_{j13}\\a_{j14}\end{bmatrix}=0,\quad [B_{Ce}]_{2\times4}\begin{bmatrix}a_{j31}\\a_{j32}\\a_{j33}\\a_{j34}\end{bmatrix}=0, \tag{29}$$

where B_{C0} and B_{Ce} are written based on equation (9):

$$B_{C0}=\begin{bmatrix}0 & 1 & 0 & 1\\ 0 & -1 & 0 & 1\end{bmatrix}$$

$$B_{Ce}=\begin{bmatrix}\sin\left(q_{j3}x^*\right) & \cos\left(q_{j3}x^*\right)\\ -E_3I_3{q_{j3}}^2\sin\left(q_{j3}x^*\right) & -E_3I_3{q_{j3}}^2\cos\left(q_{j3}x^*\right)\\ \sinh\left(q_{j3}x^*\right) & \cosh\left(q_{j3}x^*\right)\\ E_3I_3{q_{j3}}^2\sinh\left(q_{j3}x^*\right) & E_3I_3{q_{j3}}^2\cosh\left(q_{j3}x^*\right)\end{bmatrix} \tag{30}$$

where x^* is $l_1+l_2+l_3$. Also, there are four equilibrium and continuity equations relating the first part to the second and there are four more equations relating the second part to the third part:

$$[L_i]_{4\times4}\begin{bmatrix}a_{ji1}\\a_{ji2}\\a_{ji3}\\a_{ji4}\end{bmatrix}=[R_{i+1}]_{4\times4}\begin{bmatrix}a_{j(i+1)1}\\a_{j(i+1)2}\\a_{j(i+1)3}\\a_{j(i+1)4}\end{bmatrix}, \tag{31}$$

where

$$L_i=\begin{bmatrix}\sin\left(q_{ji}x^*\right) & \cos\left(q_{ji}x^*\right)\\ q_{ji}\cos\left(q_{ji}x^*\right) & -q_{ji}\sin\left(q_{ji}x^*\right)\\ -E_iI_i{q_{ji}}^2\sin\left(q_{ji}x^*\right) & -E_iI_i{q_{ji}}^2\cos\left(q_{ji}x^*\right)\\ -E_iI_i{q_{ji}}^3\cos\left(q_{ji}x^*\right) & E_iI_i{q_{ji}}^3\sin\left(q_{ji}x^*\right)\end{bmatrix}$$
$$\begin{bmatrix}\sinh\left(q_{ji}x^*\right) & \cosh\left(q_{ji}x^*\right)\\ q_{ji}\cosh\left(q_{ji}x^*\right) & q_{ji}\sinh\left(q_{ji}x^*\right)\\ E_iI_i{q_{ji}}^2\sinh\left(q_{ji}x^*\right) & E_iI_i{q_{ji}}^2\cosh\left(q_{ji}x^*\right)\\ E_iI_i{q_{ji}}^3\cosh\left(q_{ji}x^*\right) & E_iI_i{q_{ji}}^3\sinh\left(q_{ji}x^*\right)\end{bmatrix} \tag{32}$$

$$R_{i+1}=\begin{bmatrix}\sin\left(q_{j(i+1)}x^*\right)\\ q_{j(i+1)}\cos\left(q_{j(i+1)}x^*\right)\\ -E_{(i+1)}I_{(i+1)}{q_{j(i+1)}}^2\sin\left(q_{j(i+1)}x^*\right)\\ -E_{(i+1)}I_{(i+1)}{q_{j(i+1)}}^3\cos\left(q_{j(i+1)}x^*\right)\end{bmatrix}$$
$$\begin{bmatrix}\cos\left(q_{j(i+1)}x^*\right)\\ -q_{j(i+1)}\sin\left(q_{j(i+1)}x^*\right)\\ -E_{(i+1)}I_{(i+1)}{q_{j(i+1)}}^2\cos\left(q_{j(i+1)}x^*\right)\\ E_{(i+1)}I_{(i+1)}{q_{j(i+1)}}^3\sin\left(q_{j(i+1)}x^*\right)\\ \sinh\left(q_{j(i+1)}x^*\right)\\ q_{j(i+1)}\cosh\left(q_{j(i+1)}x^*\right)\\ E_{(i+1)}I_{(i+1)}{q_{j(i+1)}}^2\sinh\left(q_{j(i+1)}x^*\right)\\ E_{(i+1)}I_{(i+1)}{q_{j(i+1)}}^3\cosh\left(q_{j(i+1)}x^*\right)\\ \cosh\left(q_{j(i+1)}x^*\right)\\ q_{j(i+1)}\sinh\left(q_{j(i+1)}x^*\right)\\ E_{(i+1)}I_{(i+1)}{q_{j(i+1)}}^2\cosh\left(q_{j(i+1)}x^*\right)\\ E_{(i+1)}I_{(i+1)}{q_{j(i+1)}}^3\sinh\left(q_{j(i+1)}x^*\right)\end{bmatrix} \tag{33}$$

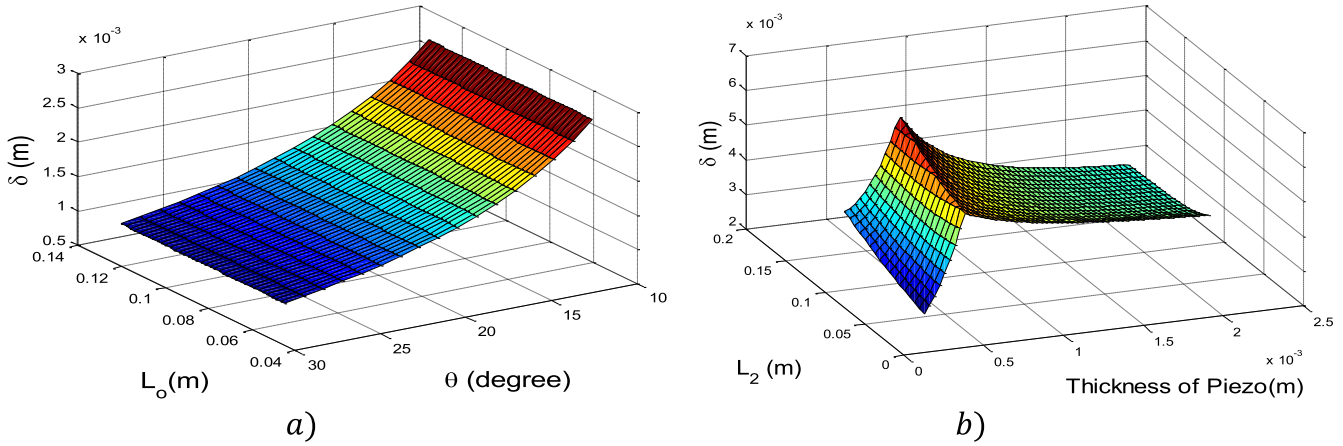

Figure 13. (a) Effect of θ angle and length of lateral beam L_0 on the gap distance in the horizontal configuration. (b) Effect of thickness and length of the piezoelectric part on the gap distance.

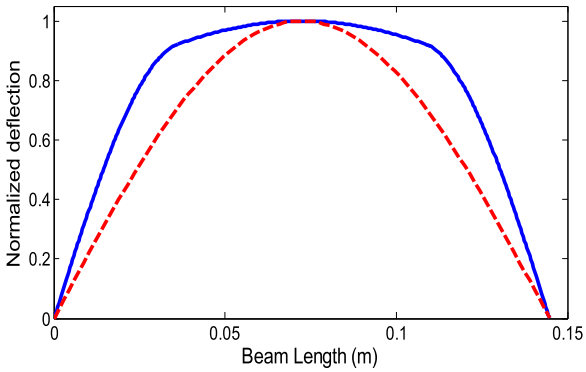

Figure 14. Deflection of a segmented beam with thick piezoelectric layer ($t_s = 0.03$ in, $t_p = 0.02$ in) versus uniform beam (dashed line).

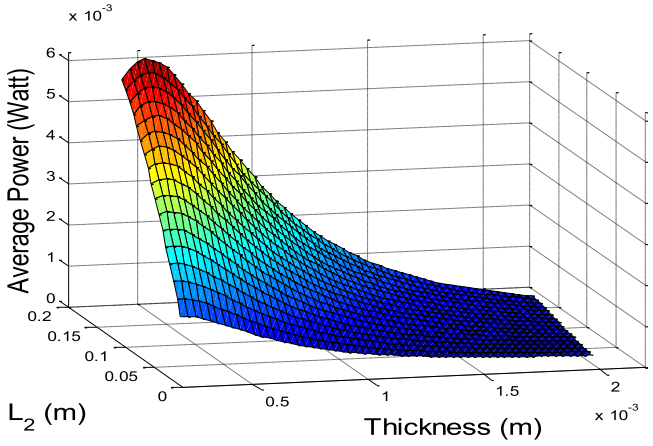

Figure 15. Effect of thickness and length of the piezoelectric (in meters) part on the average generated power (in watts).

in which

$$q_{ji} = \left(\frac{\beta_j}{\sqrt{C_i}}\right) \tag{34}$$

and x^* is l_1 or $l_1 + l_2$ or, depending on the interface we are writing the equations at. Finally we have:

$$\left[B_{C0}\right]_{2\times 4}\begin{bmatrix} a_{j11} \\ a_{j12} \\ a_{j13} \\ a_{j14} \end{bmatrix} = 0 \tag{35}$$

and

$$\left[R_3\right]^{-1}\left[L_2\right]\left[R_2\right]^{-1}\left[L_1\right]\begin{bmatrix} a_{j11} \\ a_{j12} \\ a_{j13} \\ a_{j14} \end{bmatrix} = \begin{bmatrix} a_{j31} \\ a_{j32} \\ a_{j33} \\ a_{j34} \end{bmatrix}. \tag{36}$$

If we combine equations (35) and (36) we get:

$$\begin{bmatrix} \left[B_{C0}\right]_{2\times 4} \\ \left[B_{Ce}\right]_{2\times 4}\left[\left[R_3\right]^{-1}\left[L_2\right]\left[R_2\right]^{-1}\left[L_1\right]\right]_{4\times 4} \end{bmatrix}\begin{bmatrix} a_{j11} \\ a_{j12} \\ a_{j13} \\ a_{j14} \end{bmatrix} = 0. \tag{37}$$

The matrix B is accordingly defined as:

$$B = \begin{bmatrix} \left[B_{C0}\right]_{2\times 4} \\ \left[B_{Ce}\right]_{2\times 4}\left[\left[R_3\right]^{-1}\left[L_2\right]\left[R_2\right]^{-1}\left[L_1\right]\right]_{4\times 4} \end{bmatrix}_{4\times 4}. \tag{38}$$

We find the value of β that makes the determinant of matrix B equal zero. By applying this method the size of the initial coefficient matrix (12×12) is reduced to a 4×4 matrix.

References

[1] Briand D *et al* 2015 *Micro Energy Harvesting* vol 12 (New York: Wiley)
[2] Erturk A and Inman D J 2011 *Piezoelectric Energy Harvesting* (New York: Wiley)
[3] Priya S and Inman D J 2009 *Energy Harvesting Technologies* vol 21 (Berlin: Springer)

[4] Peigney M and Siegert D 2013 Piezoelectric energy harvesting from traffic-induced bridge vibrations *Smart Mater. Struct.* **22** 095019
[5] Zuo L and Tang X 2013 Large-scale vibration energy harvesting *J. Intell. Mater. Syst. Struct.* **24** 1405–30
[6] Galchev T, McCullagh J, Peterson R and Najafi K 2011 Harvesting traffic-induced vibrations for structural health monitoring of bridges *J. Micromech. Microeng.* **21** 104005
[7] Ansari M and Karami M A 2014 Energy harvesting from controlled buckling of a horizontal piezoelectric beam *ASME 2014 Int. Design Engineering Technical Conf. and Computers and Information in Engineering Conf.* paper V008T11A017
[8] Karami M A and Inman D J 2011 Equivalent damping and frequency change for linear and nonlinear hybrid vibrational energy harvesting systems *J. Sound Vib.* **330** 5583–97
[9] Abou-Rayan A, Nayfeh A, Mook D and Nayfeh M 1993 Nonlinear response of a parametrically excited buckled beam *Nonlinear Dyn.* **4** 499–525
[10] Quinn D D, Triplett A L, Bergman L A and Vakakis A F 2011 Comparing linear and essentially nonlinear vibration-based energy harvesting *J. Vib. Acoust.* **133** 011001
[11] Daqaq M F 2010 Response of uni-modal duffing-type harvesters to random forced excitations *J. Sound Vib.* **329** 3621–31
[12] Cottone F, Vocca H and Gammaitoni L 2009 Nonlinear energy harvesting *Phys. Rev. Lett.* **102** 080601
[13] Zhou S, Cao J, Erturk A and Lin J 2013 Enhanced broadband piezoelectric energy harvesting using rotatable magnets *Appl. Phys. Lett.* **102** 173901
[14] Madankan R, Karami M A and Singla P 2014 Uncertainty analysis of energy harvesting systems *ASME 2014 Int. Design Engineering Technical Conf. and Computers and Information in Engineering Conf.* paper V006T10A066
[15] Lajnef N, Burgueño R, Borchani W, Sun Y and Heeringa A 2012 Characterization of mechanically-equivalent amplifiers and frequency modulating concepts for energy harvesting devices *ASME 2012 Conf. on Smart Materials, Adaptive Structures and Intelligent Systems* pp 897–902
[16] Cottone F, Basset P, Vocca H and Gammaitoni L 2012 Electromagnetic buckled beam oscillator for enhanced vibration energy harvesting *2012 IEEE Int. Conf. on Green Computing and Communications* (*GreenCom*) pp 624–7
[17] Cottone F, Gammaitoni L, Vocca H, Ferrari M and Ferrari V 2012 Piezoelectric buckled beams for random vibration energy harvesting *Smart Mater. Struct.* **21** 035021
[18] Zhu Y and Zu J W 2013 Enhanced buckled-beam piezoelectric energy harvesting using midpoint magnetic force *Appl. Phys. Lett.* **103** 041905
[19] Porter D A and Berfield T A 2014 A bi-stable buckled energy harvesting device actuated via torque arms *Smart Mater. Struct.* **23** 075003
[20] Masana R and Daqaq M F 2011 Electromechanical modeling and nonlinear analysis of axially loaded energy harvesters *J. Vib. Acoust.* **133** 011007
[21] Burgueño R, Hu N, Heeringa A and Lajnef N 2014 Tailoring the elastic postbuckling response of thin-walled cylindrical composite shells under axial compression *Thin-Walled Struct.* **84** 14–25
[22] Burgueno R and Lajnef N 2014 Energy harvesting devices for low frequency applications *US Patent* US20140070670 A1
[23] Burgueño R, Hu N and Lajnef N 2013 Controlling the postbuckling response of cylindrical shells under axial compression for applications in smart structures *ASME 2013 Conf. on Smart Materials, Adaptive Structures and Intelligent Systems* paper V002T07A021
[24] Daqaq M, Stabler C, Qaroush Y and Seuaciuc-Osorio T 2009 Investigation of power harvesting via parametric excitations *J. Intell. Mater. Syst. Struct.* **20** 545
[25] Stanton S C, McGehee C C and Mann B P 2010 Nonlinear dynamics for broadband energy harvesting: Investigation of a bistable piezoelectric inertial generator *Physica* D **239** 640–53
[26] Ghobadi M and Esfahani E T 2014 Foot-mounted inertial measurement unit for activity classification *2014 36th IEEE Ann. Int. Conf. in Engineering in Medicine and Biology Society* (*EMBC*) pp 6294–7
[27] Erturk A and Inman D J 2009 An experimentally validated bimorph cantilever model for piezoelectric energy harvesting from base excitations *Smart Mater. Struct.* **18** 025009
[28] Erturk A and Inman D J 2008 A distributed parameter electromechanical model for cantilevered piezoelectric energy harvesters *J. Vib. Acoust.* **130** 041002
[29] Rao S S 2007 *Vibration of Continuous Systems* (New York: Wiley)
[30] Inman D J and Singh R C 2001 *Engineering Vibration* vol 3 (Upper Saddle River, NJ: Prentice-Hall)
[31] Wu J-S 2013 *Analytical and Numerical Methods for Vibration Analyses* (New York: Wiley)
[32] Friswell M I and Adhikari S 2010 Sensor design for piezoelectric cantilever beam energy harvesters *RASD* 140–8
[33] Yamaki N and Mori A 1980 Nonlinear vibrations of a clamped beam with initial deflection and initial axial displacement: I. Theory *J. Sound Vib.* **71** 333–46
[34] Karami M A and Inman D J 2012 Controlled buckling of piezoelectric beams for direct energy harvesting from passing vehicles *ASME 2012 Int. Design Engineering Technical Conf. and Computers and Information in Engineering Conf.* pp 1231–6
[35] Erturk A, Tarazaga P A, Farmer J R and Inman D J 2009 Effect of strain nodes and electrode configuration on piezoelectric energy harvesting from cantilevered beams *J. Vib. Acoust.* **131** 011010
[36] Karami M A and Inman D J 2011 Analytical modeling and experimental verification of the vibrations of the zigzag microstructure for energy harvesting *J.Vib. Acoust.* **133** 011002